Title

Synthesis of a “Masked” Terminal Zinc Sulfide and Its Reactivity with Brønsted and Lewis Acids

Journal

Angewandte Chemie International Edition, 59(23)

ISSN

1433-7851

Authors

Cinco, Miguel Á Baeza
Wu, Guang
Kaltsoyannis, Nikolas
et al.

Publication Date

2020-06-02

DOI

10.1002/anie.202002364

Peer reviewed

Synthesis of a "Masked" Terminal Zinc Sulfide and its Reactivity with Brønsted and Lewis Acids

Miguel Á. Baeza Cinco,[a] Guang Wu,[a] Nikolas Kaltsoyannis*[b] and Trevor W. Hayton*[a]

Abstract: The "masked" terminal Zn sulfide, [K(2.2.2-cryptand][^{Me}LZn(S)] (**2**) (^{Me}L = {(2,6-^{i}Pr$_2$C$_6$H$_3$)NC(CH$_3$)}$_2$CH), was isolated via reaction of [^{Me}LZnSCPh$_3$] (**1**) with 2.3 equiv of KC$_8$ in THF, in the presence of 2.2.2-cryptand, at –78 °C. Complex **2** reacts readily with PhCCH and N$_2$O to form [K(2.2.2-cryptand)][^{Me}LZn(SH)(CCPh)] (**4**) and [K(2.2.2-cryptand)][^{Me}LZn(SNNO)] (**5**), respectively, displaying both Brønsted and Lewis basicity. In addition, the electronic structure of **2** was examined computationally and compared with the previously reported Ni congener, [K(2.2.2-cryptand)][^{tBu}LNi(S)] (^{tBu}L = {(2,6-^{i}Pr$_2$C$_6$H$_3$)NC(^{t}Bu)}$_2$CH).

Introduction

Transition metal oxo complexes have been the subject of intense scrutiny over the past four decades owing to their intermediacy in a wide array of processes, from biological to industrial.[1–6] Despite these efforts, the isolation of late metal (i.e., beyond group 8) terminal oxos has proven challenging - a consequence of the "oxo wall".[7] This concept postulates that a terminal oxo in a tetragonal field with a >d^5 configuration will not be isolable because of the occupation of M=O π* molecular orbitals. In line with this premise, all known late metal oxo/imido/nitrido complexes feature reduced coordination numbers, which liberates d orbitals to host non-bonding electrons. Examples include Wilkinson's four-coordinate Ir oxo [Mes$_3$Ir(O)] (Mes = 2,4,6-Me$_3$C$_6$H$_2$),[8] a four-coordinate Co oxo [PhB(^{t}BuIm)$_3$Co(O)] (^{t}BuIm = 3-^{t}Bu-imidazolyl),[9] and more recently the four-coordinate Ir oxo [(PNP)Ir(O)] (PNP = N(CHCHP^{t}Bu$_2$)$_2$),[10] among others.[11–13]

A similar electronic picture arises for the heavier sulfur congeners. Indeed, the only isolated examples, a family of "masked" Ni sulfides [K(L)][^{R}LNi(S)] (^{R}L = {(2,6-^{i}Pr$_2$C$_6$H$_3$)NC(R)}$_2$CH; R = Me, ^{t}Bu; L = 18-crown-6, 2.2.2-cryptand) reported by our group, all feature trigonal coordination environments at Ni.[14] These complexes contain a highly reactive [Ni=S]$^-$ fragment, which can activate a wide variety of small molecules, including N$_2$O, NO, CO, CS$_2$, and CO$_2$.[14–17] We accessed these Ni sulfide complexes via reductive removal of a trityl protecting group. In fact, this "reductive deprotection" reaction has proven to be broadly useful for the synthesis of M=E mulitple bonds, and we have used this approach to successfully synthesize a series of terminal actinide chalcogenides, [K(18-crown-6)][An(E)(NR$_2$)$_3$] (An = Th, U; E = O, S; R = SiMe$_3$), as well as the aforementioned Ni sulfides.[14,18,19]

Going forward, we were interested in understanding the extent of π bonding within the [Ni=S]$^-$ fragment. In this regard, the isostructural zinc sulfide, which features a closed shell d^{10} metal ion, offers a useful comparison with the Ni analogue, because of its inability to engage in π bonding. Herein, we report the successful synthesis and structural characterization of a "masked" terminal Zn sulfide via reductive deprotection, as well as a preliminary reactivity profile. Moreover, in an effort to better understand these systems, the [Zn–S]$^+$ fragment was probed by DFT/NBO/QTAIM analysis and compared with the [Ni=S]$^-$ fragment in [K(2.2.2-cryptand)][^{tBu}LNi(S)], as well as the isolated anion [^{Me}LNi(S)]$^-$.

Results and Discussion

Addition of 1 equiv of KSCPh$_3$ to [^{Me}LZnCl][20] in THF results in the formation of [^{Me}LZn(SCPh$_3$)] (**1**), which can be isolated in 85 % yield after work-up (Scheme 1). In the solid state, **1** crystallizes with two independent molecules in the asymmetric unit (Figure S21) and its metrical parameters mirror those found in the closely related Zn trityl thiolate, [^{Me*}LZn(SCPh$_3$)] (^{Me*}L = {(2,6-(CH$_3$)$_2$C$_6$H$_3$)NC(CH$_3$)}$_2$CH), reported by Warren and co-workers.[21] For instance, the Zn–S distances in **1** are 2.212(3) and 2.191(3) Å, whereas this distance in

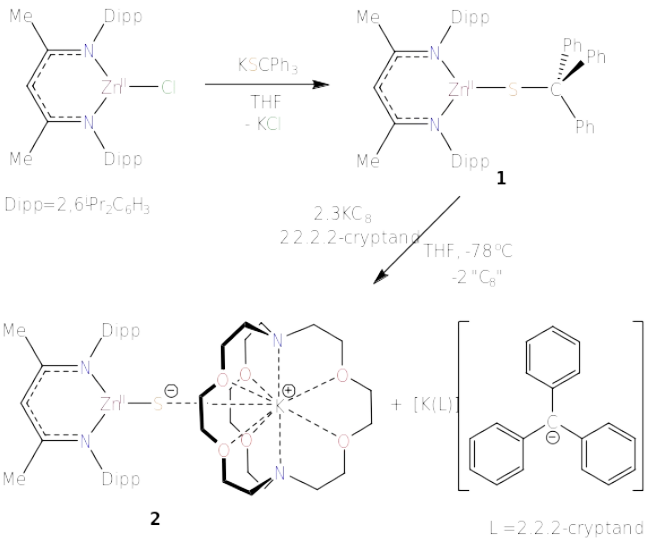

Scheme 1. Synthesis of complexes **1** and **2**.

[a] M. A. Baeza Cinco, Dr. G. Wu, Prof. Dr. T. W. Hayton
Department of Chemistry and Biochemistry
University of California, Santa Barbara
Santa Barbara, CA 93016 (USA)
E-mail: hayton@chem.ucsb.edu
[b] Prof. Dr. N. Kaltsoyannis
Department of Chemistry
University of Manchester
Oxford Road
Manchester M13 9PL (UK)
E-mail: nikolas.kaltsoyannis@manchester.ac.uk
Supporting information for this article is given via a link at the end of the document.

[^{Me*}LZn(SCPh$_3$)] is 2.2142(6) Å. In addition, complex **1** has been characterized by ^{1}H and ^{13}C{^{1}H} NMR spectroscopies and elemental analysis. It is stable for months when stored as a solid under an inert atmosphere at –24 °C.

Next, we applied the reductive deprotection methodology to **1**, in an attempt to synthesize a terminal Zn sulfide via selective C–S bond cleavage. Thus, addition of 2.3 equiv of KC_8 to **1** in the presence of 2.2.2-cryptand in THF at –78 °C results in immediate formation of a deep red suspension, signalling release of the trityl anion, [K(2.2.2-cryptand)][CPh$_3$]. Work-up of the reaction mixture after 10 min enables the isolation of [K(2.2.2-cryptand][^{Me}LZn(S)] (**2**), which can be isolated as a yellow crystalline solid in 47% yield (Scheme 1). Complex **2** has been characterized by X-ray crystallography, ^{1}H and ^{13}C{^{1}H} NMR spectroscopies, IR and UV-vis spectroscopies, and elemental analysis. Its crystallizes in the non-centrosymmetric space group Cc as the Et_2O solvate, **2**·Et_2O, with four independent molecules in the asymmetric unit (Figure 1). The

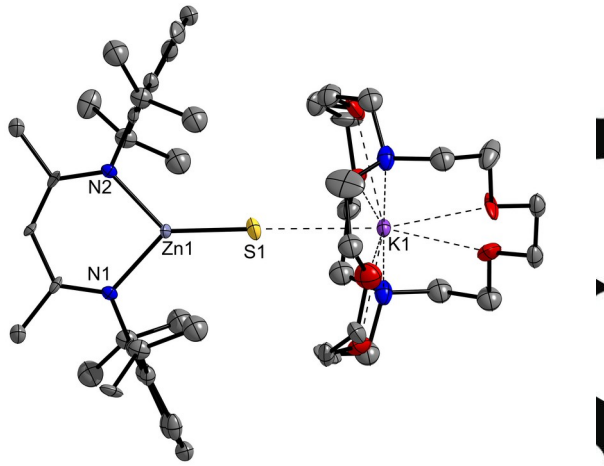

Figure 1. Molecular structure of **2**·Et_2O. Thermal ellipsoids shown at 50% probability. Et_2O solvates, hydrogen atoms, and three other molecules in the asymmetric unit omitted for clarity.

metrical parameters of all four molecules are similar, and only the average values will be discussed. The solid-state structure of **2** features a trigonal planar geometry around the Zn center (ΣL-Zn-L = 359.8°), as well as a remarkably short av. Zn–S bond length of 2.107 Å (range: 2.083(5)–2.148(5) Å). We ascribe this short distance to the electrostatic contraction originating from the high charge on the S atom. For comparison, the bridging Zn sulfide complex, [{HB(3-*p*-cumenyl-5-methylpyrazolyl)$_3$}Zn]$_2$(μ-S),[22] has a Zn–S bond length of 2.186(2) Å, while the two-coordinate Zn dithiolate complex, [(2,6-^{i}Pr$_2$C$_6$H$_3$S)$_2$Zn,[23] has a Zn–S distance of 2.159(6) Å.

A comparison of **2** with its Ni analogue, [K(2.2.2-cryptand)][^{tBu}LNi(S)] is also informative (Table 1). Surprisingly, its M–S bond length (2.084(1) Å) is comparable to those of **2**, despite the nominally higher bond order in the Ni example. However, complex **2** possesses a shorter average S···K distance (3.115 Å) than that observed for [K(2.2.2-cryptand)][^{tBu}LNi(S)] (3.379(1) Å), consistent with the higher predicted charge density at the S^{2-} ligand in **2**. That said, the S···K interaction in **2** is still quite long, suggesting that it can also be considered a "masked" terminal sulfide.

Table 1. Selected bond lengths and bond angles for the masked sulfides **2**·Et_2O and [K(2.2.2-cryptand)][^{tBu}LNi(S)]. Average values shown for **2**·Et_2O. Computed (DFT) data in italics. For M–S, the second italicized number refers to the distance in the isolated anions [^{R}LM(S)]$^-$ (R = Me, M = Zn; R = ^{t}Bu, M = Ni).

Bond/ angle	**2**·Et_2O	[K(2.2.2-cryptand)] [^{tBu}LNi(S)]
M–S (Å)	2.107 *2.148, 2.109*	2.084(1) *2.095, 2.060*
S···K (Å)	3.115 *3.123*	3.379(1) *3.349*
av. M–N (Å)	2.098 *2.064*	1.93 *1.973*
M–S–K (°)	169.45 *176.4*	170.08(5) *177.1*

Complex **2** is soluble in benzene, toluene, Et_2O, DME, THF, and pyridine, but insoluble in hexanes and pentane. Although **2** can be isolated in analytically pure form and has been fully characterized, it is relatively unstable. For example, THF solutions of **2** completely decompose over the course of 3 d, depositing a colourless solid. An X-ray crystallographic analysis identified the main decomposition product as the tetrametallic zinc sulfide, [K(2.2.2-cryptand)]$_2$[^{Me}LZn(μ-S)(μ-S)Zn]$_2$ (**3**·2THF), which features a "ladder-like" Zn_4S_4 core formed by oligomerization of 4 equiv of **2**, concomitant with apparent release of 2 equiv of [K(2.2.2-cryptand)][^{Me}L] (See SI). For comparison, [K(2.2.2-cryptand)][^{tBu}LNi(S)] features much higher thermal stability, suggesting that the sulfide ligand in **2** is more reactive, as anticipated.

To better understand the bonding within the [M–S]$^-$ fragment (M = Zn, Ni) we turned to hybrid density functional theory (PBE0). We examined the masked platforms **2** and [K(2.2.2-cryptand][^{tBu}LNi(S)], as well as their isolated anionic components, i.e., [^{R}LM(S)]$^-$ (R = Me, M = Zn; R = ^{t}Bu, M = Ni). The computed electronic structures were studied using the Natural Bond Orbital (NBO) and Quantum Theory of Atoms-in-Molecules (QTAIM) approaches. Natural atomic charges and M–S Wiberg Bond Indices (WBIs) are collected in Table 2, and details of the M–S Natural Localized Molecular Orbitals (NLMOs) are given in Table S1 and Figures S1-S12. Note that both the isolated and masked anions for the Ni analogue were calculated in their triplet state (the lowest singlet state of the isolated anion was found to be 51.2 kJ/mol less stable than the triplet, and the electronic structure of the quintet failed to converge). Minimal spin contamination was found in both Ni systems, with $\langle S^2 \rangle$ = 2.03 for [^{tBu}LNi(S)]$^-$ and 2.02 for [K(2.2.2-cryptand][^{tBu}LNi(S)].

Both the isolated anion, [^{Me}LZn(S)]$^-$, and **2** have a single Zn–S σ bonding NLMO, which is mainly S3p in character. The remaining two S3p orbitals correspond to the sulfur lone pairs. These orbitals do not interact with the Zn center, consistent with the $3d^{10}$ configuration of Zn^{2+} (Figure 2). Additionally, **2** features a somewhat smaller Zn–S WBI than in the isolated anion, reflecting its slightly longer bond length (Table 1). This is also the case for the QTAIM delocalisation indices (Table 2), although the absolute values of these bond order measures are significantly larger than the analogous WBIs. For both Zn–S bonds, the QTAIM ellipticities at the bond critical point are very close to zero (Table 2), as expected for a cylindrically symmetrical interaction, and are consistent with a formal bond order of 1.

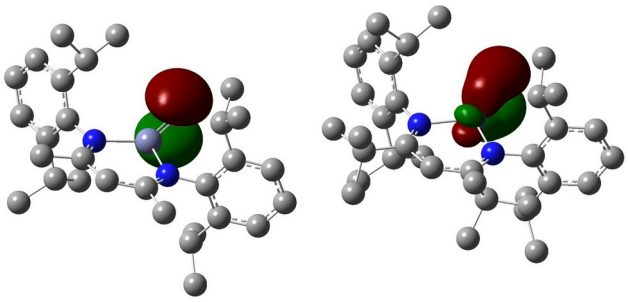

Figure 2. Comparison the S3p$_\perp$ orbital (NLMO 56) in [^{Me}LZn(S)]$^-$ vs. the Ni–S $\pi_\perp$ orbital (NLMO 155β) in [^{tBu}LNi(S)]$^-$. Isosurface value = 0.05. Hydrogen atoms omitted for clarity.

In [^{tBu}LNi(S)]$^-$, there are five α spin and three β spin Ni 3d-based orbitals, as expected for a Ni^{2+} d^8 configuration. There is also an α spin Ni-S σ NLMO, which is similar in composition to the Zn equivalent, although the metal component, which is predominantly s in character, is reduced in the Ni system (14.2% *vs* 21.3% for Zn). There is a β spin equivalent of this NLMO. In addition, there are two β spin Ni–S π NLMOs, which have more metal content (40.0% and 24.7%) than the S orbitals and are Ni3d/S3p in character (Figure 2). The Ni–S WBI and δ values are both significantly larger than in [^{Me}LZn(S)]$^-$, reflecting the π bonding in the Ni system and a formal M–S bond order of 2. The presence of two orthogonal β spin π orbitals accounts for the bond critical point ellipticity remaining close to zero. The Ni–S bonding in [K(2.2.2-cryptand)][^{tBu}LNi(S)] is similar: one α spin σ NLMO, and σ + 2π in the β spin manifold. The NLMOs are generally more S-localised in [K(2.2.2-cryptand)][^{tBu}LNi(S)] than the anion alone, as a result of the slightly longer M–S bond, and the WBI and δ are smaller, as in the Zn systems.

Table 2. Natural atomic charges *q*, M–S Wiberg Bond Indices *WBI*, M–S delocalisation indices δ and ellipticities at the M–S bond critical point ε for [^{Me}LZn(S)]$^-$, [K(2.2.2-cryptand)][^{Me}LZn(S)] (**2**), [^{tBu}LNi(S)]$^-$ and [K(2.2.2-cryptand)][^{tBu}LNi(S)].

	q_M	q_S	*WBI*	δ	ε
[^{Me}LZn(S)]$^-$	1.38	-1.45	0.68	1.20	0.01
[K(2.2.2-cryptand)][^{Me}LZn(S)] (**2**)	1.48	-1.52	0.51	1.03	0.02
[^{tBu}LNi(S)]$^-$	0.88	-1.04	1.18	1.57	0.04
[K(2.2.2-cryptand)][^{tBu}LNi(S)]	1.04	-1.22	0.95	1.34	0.02

As noted above, the experimental S···K distance is significantly longer in [K(2.2.2-cryptand)][^{tBu}LNi(S)] than in **2**, attributed to higher charge density at S. The difference in the calculated S···K distances between the two masked systems is not as large as seen experimentally, but that in the Ni complex is 0.126 Å longer than in **2** (Table 1). Finally, Table 2 shows that the Natural charge of the S atom is indeed more negative in **2** than in [K(2.2.2-cryptand)][^{tBu}LNi(S)], which may account for its greater reactivity.

We next explored the reactivity of **2** towards electrophiles. Reaction of **2** with 1 equiv of PhCCH in toluene resulted in formation of a new C_s-symmetric product, as revealed by ^{1}H NMR spectroscopic monitoring of the reaction. Work-up of the reaction mixture resulted in isolation of [K(2.2.2-cryptand)][^{Me}LZn(SH)(CCPh)] (**4**), which was formed by protonation of the Zn–S bond of **2** by PhCCH (Scheme 2). Complex **4** can be isolated as large colorless plates in 41 % yield as the THF solvate, **4**·2THF. This reaction clearly illustrates the potent basicity of **2**, especially relative to [K(18-crown-6)][^{tBu}LNi(S)], which does not react with PhCCH.

Complex **4**·2THF crystallizes in the monoclinic space group $P2_1/n$ (Figure 3). In the solid state, the Zn ion adopts a pseudo-tetrahedral geometry (τ_4 = 0.928),[24] and is bound by a β-diketiminate ligand, a hydrosulfide ligand, and a phenylacetylide ligand. The structure also possesses an outer sphere [K(2.2.2-cryptand)]$^+$ cation. The Zn–S bond length (2.332(3) Å) is substantially longer than the Zn–S distance observed in **2**, as expected. The Zn–C distance in **4** (2.021(5) Å) is similar to that in other Zn acetylide complexes, such as α-diimine-supported [LZn(CCPh)$_2$] (Zn–C = 1.966(3), 1.953(3) Å) (L = {(2,6-^{i}Pr$_2$C$_6$H$_3$)NC(CH$_3$)}$_2$), and the homoleptic acetylide, K$_2$[Zn(CCPh)$_4$] (av. Zn–C = 2.0475 Å).[25] The ^{1}H NMR spectrum of **4** is consistent with the C_s symmetry observed in the solid state; for instance, its ^{1}H NMR spectrum shows two inequivalent ^{i}Pr environments. In addition, the hydrosulfide S–H resonance was observed at δ = -2.45 ppm, further confirming our formulation. This value is similar to those of other Zn hydrosulfides.[22,26,27] Finally, we observe the $\nu_{C\equiv C}$ mode in **4** at 2096 cm^{-1} (Figure S27).

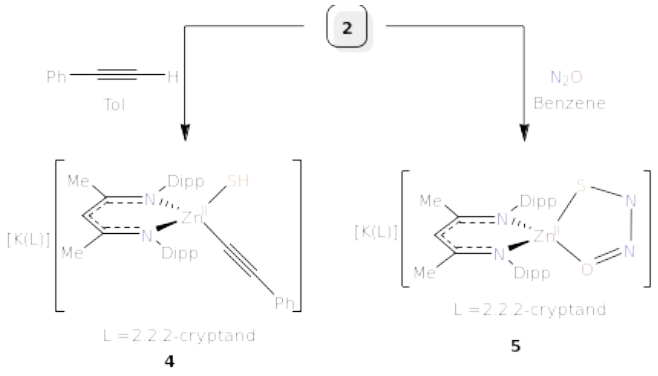

Scheme 2. Synthesis of complexes **4** and **5**.

Exposure of complex **2** to 1 atm of N_2O results in rapid formation of the thiohyponitrite complex, [K(2.2.2-cryptand)][^{Me}LZn(SNNO)] (**5**) (Scheme 2), which can be isolated as a colorless crystalline solid in 54 % yield. Complex **5** is only the second example of a thiohyponitrite complex, the first being formed from the analogous reaction of N_2O with [K(18-crown-6)][^{tBu}LNi(S)].[14] It is worth noting that the reaction of complex **2** with N_2O reaches completion almost immediately (< 4 min), whereas the reaction of N_2O with the isostructural Ni sulfide complex requires ca. 3 hr to reach completion. The Zn center in **5**·2.5C_6H_6 features a distorted tetrahedral geometry (τ_4 = 0.773)[24] that is bound with a κ^2 *cis*-thiohyponitrite ligand and the β-diketiminate ligand, displaying overall C_s symmetry (Figure 3). The O–N and N–N distances in **5** are 1.229(6) Å and 1.306(7) Å, respectively. Curiously, these values are much different than those observed for [K(18-crown-6)][^{tBu}LNi(SNNO)]. For example, the O–N and N–N distances in [K(18-crown-6)][^{tBu}LNi(SNNO)] are 1.308(3) Å and 1.154(9) Å, respectively. Likewise, longer and shorter O–N and N–N distances, respectively, are found in most other hyponitrite complexes, including [$(PPh_3)_2$Pt(O_2N_2)] (av. O–N = 1.37 Å, N–N = 1.23 Å),[30] {[Fe$(NO)_2]_2$(μ-bdmap)}$_2$(κ^4-N_2O_2) (bdmap = 1,3-bis(dimethylamino)-2-propanolate; O–N = 1.330(3) Å, N–N = 1.279(5) Å),[29] and K_2[(NON)Al(η^2-O_2N_2)]$_2$ (NON = 4,5-bis(2,6-^{i}Pr$_2$-anilido)-2,7-^{t}Bu$_2$-9,9-dimethylxanthene; av. O-N = 1.378 Å, N–N = 1.251(3) Å),[31] among others.[31–34] Overall, the structural features observed for **5**, especially the N–N distance, suggest a contribution of the [SNN=O]$^{2-}$ resonance form to the overall electronic structure, in addition to the expected [EN=NO]$^{2-}$ (E = O, S) resonance form observed previously for the (thio)hyponitrite ligand. Complex **5** also possesses Zn–O and Zn–S distances of 1.977(2) Å and 2.226(2) Å, respectively. These values fall within the expected range for the Zn^{2+} ion.[35–40]

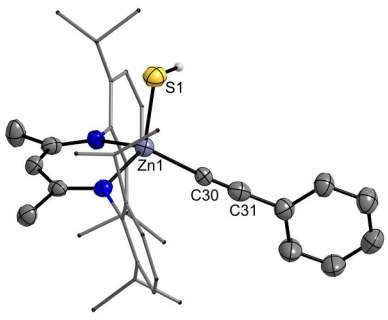

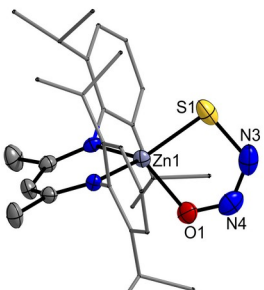

Figure 3. Molecular structures of **4**·THF (top) and **5**·2.5C_6H_6 (bottom). Thermal ellipsoids shown at 50% probability. Except for the hydrosulfide proton in **4**, all hydrogen atoms omitted for clarity. Solvate molecules and [K(2.2.2-cryptand)]$^+$ cations omitted for clarity.

The ^{1}H NMR spectrum of **5** features signals assignable to a single ^{i}Pr environment for the β-diketiminate ligand (Figure S20), as evidenced by the diastereotopic methyl resonances at 1.59 and 1.33 ppm. The ^{1}H NMR spectrum of **5** argues for a C_{2v}-symmetric complex in solution, which contrasts with the C_s symmetry observed in the solid state. To explain this observation, we suggest that the thiohyponitrite ligand can adopt a fluxional mode, which allows it to rotate within the β-diketiminate binding pocket. We hypothesize that the apparent low barrier of exchange is due to the additional contribution of the [SNN=O]$^{2-}$ resonance form. Further NMR characterization of **5** was hampered by its poor solubility or instability in most solvents. Intriguingly, however, when **5** was dissolved in pyridine-d_5, it converted into **3**, suggesting that N_2O addition to **2** is reversible under some conditions.

Conclusions

In conclusion, we synthesized and characterized the first "masked" terminal zinc sulfide, [K(2.2.2-cryptand)][^{Me}LZn(S)], via reductive deprotection of the Zn trityl thiolate complex, [^{Me}LZn(SCPh$_3$)]. [K(2.2.2-cryptand)][^{Me}LZn(S)] is among a growing number of chalcogenide complexes,[41–44] such as the recently isolated molecular Al oxides K_2[(NON)Al(O)(THF)]$_2$ and K_2[(^{Ar}NON)Al(O)]$_2$ (^{Ar}NON = [O(SiMe$_2$NAr)$_2$]$^{2-}$, Ar = 2,6-^{i}Pr$_2$C$_6$H$_3$), as well as the in-situ generated Ga oxide [^{Me}LGa(O)],[30,34,45] which feature minimal (if any) M–E π-bonding. Indeed, our Natural Localised Molecular Orbital analysis finds only a Zn–S σ bond in both [K(2.2.2-cryptand)][^{Me}LZn(S)] and its anionic fragment, [^{Me}LZn(S)]$^-$. By contrast, the Ni–S σ bonding in the isostructural Ni complex, [K(2.2.2-cryptand)][^{tBu}LNi(S)], is augmented by two β spin Ni–S π orbitals. Moreover, our DFT analysis confirms the predicted stronger polarization within the Zn–S bond, in accordance with experimental observations. The decrease in bond order on moving from the Ni to Zn analogue is important confirmation of the central tenet of the "oxo wall" postulate. Intriguingly, though, the M–S bond lengths within these two fragments are essentially identical, despite their fundamentally different bonding schemes (Δ_{M-S} = 0.023 Å).

Finally, we found that [K(2.2.2-cryptand)][^{Me}LZn(S)] can deprotonate PhCCH to produce [K(2.2.2-cryptand)][^{Me}LZn(SH)(CCPh)] and, more remarkably, capture N_2O, forming the thiohyponitrite complex, [K(2.2.2-cryptand)][^{Me}LZn(SNNO)], which contains a rare example of an

$[SNNO]^{2-}$ ligand. These reactions clearly outline the potent reactivity of the sulfide ligand in [K(2.2.2-cryptand][^{Me}LZn(S)], which can function as both a strong Brønsted and Lewis base. Further reactivity studies with other small molecules are currently underway.

Acknowledgements

This work was supported by the National Science Foundation (CHE 1764345). NMR spectra were collected on instruments supported by an NIH Shared Instrumentation Grant (SIG, 1S10OD012077-01A1). We are grateful to the University of Manchester's Computational Shared Facility for computational resources and associated services.

Keywords: zinc • sulfides • nitrogen oxides • protecting groups • multiple bonding

[1] J. Rittle, M. T. Green, *Science* **2010**, *330*, 933–937.
[2] M. Sono, M. P. Roach, E. D. Coulter, J. H. Dawson, *Chem. Rev.* **1996**, *96*, 2841–2888.
[3] Y. Surendranath, M. W. Kanan, D. G. Nocera, *J. Am. Chem. Soc.* **2010**, *132*, 16501–16509.
[4] R. Gupta, T. Taguchi, B. Lassalle-Kaiser, E. L. Bominaar, J. Yano, M. P. Hendrich, A. S. Borovik, *Proc. Natl. Acad. Sci.* **2015**, *112*, 5319–5324.
[5] S. Yoshikawa, A. Shimada, *Chem. Rev.* **2015**, *115*, 1936–1989.
[6] M. Wikström, K. Krab, V. Sharma, *Chem. Rev.* **2018**, *118*, 2469–2490.
[7] J. R. Winkler, H. B. Gray, in *Mol. Electron. Struct. Transit. Met. Complexes I* (Eds.: D.M.P. Mingos, P. Day, J.P. Dahl), Springer, Berlin, Heidelberg, **2012**, pp. 17–28.
[8] R. S. Hay-Motherwell, G. Wilkinson, B. Hussain-Bates, M. B. Hursthouse, *Polyhedron* **1993**, *12*, 2009–2012.
[9] M. K. Goetz, E. A. Hill, A. S. Filatov, J. S. Anderson, *J. Am. Chem. Soc.* **2018**, *140*, 13176–13180.
[10] D. Delony, M. Kinauer, M. Diefenbach, S. Demeshko, C. Würtele, M. C. Holthausen, S. Schneider, *Angew. Chem. Int. Ed.* **2019**, *58*, 10971–10974.
[11] E. Poverenov, I. Efremenko, A. I. Frenkel, Y. Ben-David, L. J. W. Shimon, G. Leitus, L. Konstantinovski, J. M. L. Martin, D. Milstein, *Nature* **2008**, *455*, 1093–1096.
[12] S. Hong, F. F. Pfaff, E. Kwon, Y. Wang, M.-S. Seo, E. Bill, K. Ray, W. Nam, *Angew. Chem. Int. Ed.* **2014**, *53*, 10403–10407.
[13] E. Andris, R. Navrátil, J. Jašík, M. Srnec, M. Rodríguez, M. Costas, J. Roithová, *Angew. Chem. Int. Ed.* **2019**, *58*, 9619–9624.
[14] N. J. Hartmann, G. Wu, T. W. Hayton, *Angew. Chem. Int. Ed.* **2015**, *54*, 14955–14959.
[15] N. J. Hartmann, G. Wu, T. W. Hayton, *J. Am. Chem. Soc.* **2016**, *138*, 12352–12355.
[16] N. J. Hartmann, G. Wu, T. W. Hayton, *Dalton Trans.* **2016**, *45*, 14508–14510.
[17] N. J. Hartmann, G. Wu, T. W. Hayton, *Organometallics* **2017**, *36*, 1765–1769.
[18] D. E. Smiles, G. Wu, N. Kaltsoyannis, T. W. Hayton, *Chem. Sci.* **2015**, *6*, 3891–3899.
[19] D. E. Smiles, G. Wu, T. W. Hayton, *J. Am. Chem. Soc.* **2014**, *136*, 96–99.
[20] J. Prust, A. Stasch, W. Zheng, H. W. Roesky, E. Alexopoulos, I. Usón, D. Böhler, T. Schuchardt, *Organometallics* **2001**, *20*, 3825–3828.
[21] M. S. Varonka, T. H. Warren, *Inorganica Chim. Acta* **2007**, *360*, 317–328.
[22] M. Ruf, H. Vahrenkamp, *Inorg. Chem.* **1996**, *35*, 6571–6578.
[23] J. Pratt, A. M. Bryan, M. Faust, J. N. Boynton, P. Vasko, B. D. Rekken, A. Mansikkamäki, J. C. Fettinger, H. M. Tuononen, P. P. Power, *Inorg. Chem.* **2018**, *57*, 6491–6502.
[24] L. Yang, D. R. Powell, R. P. Houser, *Dalton Trans.* **2007**, 955–964.
[25] J. Gao, S. Li, Y. Zhao, B. Wu, X.-J. Yang, *Organometallics* **2012**, *31*, 2978–2985.
[26] M. Rombach, H. Vahrenkamp, *Inorg. Chem.* **2001**, *40*, 6144–6150.
[27] A. Looney, R. Han, I. B. Gorrell, M. Cornebise, K. Yoon, G. Parkin, A. L. Rheingold, *Organometallics* **1995**, *14*, 274–288.
[28] N. Arulsamy, D. S. Bohle, J. A. Imonigie, R. C. Moore, *Polyhedron* **2007**, *26*, 4737–4746.
[29] W.-Y. Wu, C.-N. Hsu, C.-H. Hsieh, T.-W. Chiou, M.-L. Tsai, M.-H. Chiang, W.-F. Liaw, *Inorg. Chem.* **2019**, *58*, 9586–9591.
[30] J. Hicks, M. Heilmann, P. Vasko, J. M. Goicoechea, S. Aldridge, *Angew. Chem.* **2019**, *131*, 17425–17428.
[31] D. Beck, P. Knüpfer, *Chem. – Eur. J.* **2018**, *24*, 16019–16028.
[32] D. Pinelli, G. de Ruiter, T. Agapie, *J. Am. Chem. Soc.* **2016**, *138*, 5008–5011.
[33] S. C. Puiu, T. H. Warren, *Organometallics* **2003**, *22*, 3974–3976.
[34] M. D. Anker, M. P. Coles, *Angew. Chem. Int. Ed.* **2019**, *58*, 18261–18265.
[35] M. Tahmassebimehr, A. Decortes, S. M. Al-Amsyar, W. Lueangchaichaweng, C. J. Whiteoak, E. C. Escudero-Adán, A. W. Kleij, P. P. Pescarmona, *Catal. Sci. Technol.* **2012**, *2*, 2231–2237.
[36] N. Chopin, M. Médebielle, G. Pilet, *J. Fluor. Chem.* **2013**, *155*, 89–96.
[37] C. Zhang, Z.-X. Wang, *J. Organomet. Chem.* **2008**, *693*, 3151–3158.
[38] A. Schneider, H. Vahrenkamp, *Z. Für Anorg. Allg. Chem.* **2003**, *629*, 2122–2126.
[39] F. E. Jacobsen, S. M. Cohen, *Inorg. Chem.* **2004**, *43*, 3038–3047.
[40] M. Ji, B. Benkmil, H. Vahrenkamp, *Inorg. Chem.* **2005**, *44*, 3518–3523.
[41] D. Franz, S. Inoue, *Dalton Trans.* **2016**, *45*, 9385–9397.
[42] T. Chu, S. F. Vyboishchikov, B. Gabidullin, G. I. Nikonov, *Angew. Chem. Int. Ed.* **2016**, *55*, 13306–13311.
[43] M. D. Anker, M. P. Coles, *Angew. Chem. Int. Ed.* **2019**, *58*, 13452–13455.
[44] D. Franz, T. Szilvási, E. Irran, S. Inoue, *Nat. Commun.* **2015**, *6*, 1–6.
[45] A. Kassymbek, S. F. Vyboishchikov, B. M. Gabidullin, D. Spasyuk, M. Pilkington, G. I. Nikonov, *Angew. Chem. Int. Ed.* **2019**, *58*, 18102–18107.

Entry for the Table of Contents

RESEARCH ARTICLE

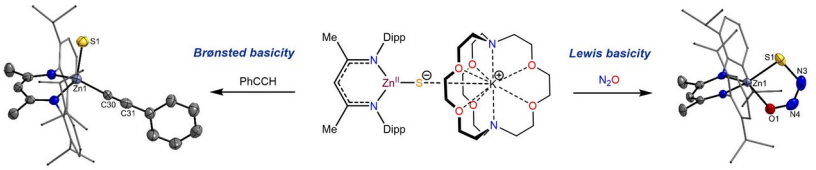

The “masked“ terminal Zn sulfide, [K(2.2.2-cryptand][^{Me}LZn(S)] (^{Me}L = {(2,6-^{i}Pr$_2$C$_6$H$_3$)NC(CH$_3$)}$_2$CH), displays high Brønsted and Lewis basicity in its reactions with phenylacetylene and nitrous oxide, respectively.

Miguel Á. Baeza Cinco, Guang Wu, Nikolas Kaltsoyannis and Trevor W. Hayton**

Page No. – Page No.

Synthesis of a “Masked” Terminal Zinc Sulfide and its Reactivity with Brønsted and Lewis Acids